APPLIED AND ENVIRONMENTAL MICROBIOLOGY, Feb. 2010, p. 900–909 Vol. 76, No. 3
0099-2240/10/$12.00 doi:10.1128/AEM.02337-09

Aggregate Size and Architecture Determine Microbial Activity Balance for One-Stage Partial Nitritation and Anammox▽

Siegfried E. Vlaeminck,[1] Akihiko Terada,[2]† Barth F. Smets,[2] Haydée De Clippeleir,[1] Thomas Schaubroeck,[1] Selin Bolca,[1] Lien Demeestere,[3] Jan Mast,[3] Nico Boon,[1] Marta Carballa,[1]‡ and Willy Verstraete[1]*

Laboratory of Microbial Ecology and Technology (LabMET), Ghent University, Coupure Links 653, 9000 Ghent, Belgium[1]; Department of Environmental Engineering, Technical University of Denmark (DTU), Miljoevej, Building 113, 2800 Kongens Lyngby, Denmark[2]; and Veterinary and Agrochemical Research Centre (VAR), Groeselenberg 99, 1180 Brussels, Belgium[3]

Received 28 September 2009/Accepted 23 November 2009

Aerobic ammonium-oxidizing bacteria (AerAOB) and anoxic ammonium-oxidizing bacteria (AnAOB) cooperate in partial nitritation/anammox systems to remove ammonium from wastewater. In this process, large granular microbial aggregates enhance the performance, but little is known about granulation so far. In this study, three suspended-growth oxygen-limited autotrophic nitrification-denitrification (OLAND) reactors with different inoculation and operation (mixing and aeration) conditions, designated reactors A, B, and C, were used. The test objectives were (i) to quantify the AerAOB and AnAOB abundance and the activity balance for the different aggregate sizes and (ii) to relate aggregate morphology, size distribution, and architecture putatively to the inoculation and operation of the three reactors. A nitrite accumulation rate ratio (NARR) was defined as the net aerobic nitrite production rate divided by the anoxic nitrite consumption rate. The smallest reactor A, B, and C aggregates were nitrite sources (NARR, >1.7). Large reactor A and C aggregates were granules capable of autonomous nitrogen removal (NARR, 0.6 to 1.1) with internal AnAOB zones surrounded by an AerAOB rim. Around 50% of the autotrophic space in these granules consisted of AerAOB- and AnAOB-specific extracellular polymeric substances. Large reactor B aggregates were thin film-like nitrite sinks (NARR, <0.5) in which AnAOB were not shielded by an AerAOB layer. Voids and channels occupied 13 to 17% of the anoxic zone of AnAOB-rich aggregates (reactors B and C). The hypothesized granulation pathways include granule replication by division and budding and are driven by growth and/or decay based on species-specific physiology and by hydrodynamic shear and mixing.

In the last few years, autotrophic nitrogen removal via partial nitritation and anoxic ammonium oxidation (anammox) has evolved from lab- to full-scale treatment of nitrogenous wastewaters with a low biodegradable organic compound content, and this evolution has been driven mainly by a significant decrease in the operational costs compared to the costs of conventional nitrification and heterotrophic denitrification (11, 23). Oxygen-limited autotrophic nitrification and denitrification (OLAND) is one of the autotrophic processes used and is a one-stage procedure; i.e., partial nitritation and anammox occur in the same reactor (30). The "functional" autotrophic microorganisms in OLAND include aerobic ammonium-oxidizing bacteria (AerAOB) and anoxic ammonium-oxidizing bacteria (AnAOB). With oxygen, AerAOB oxidize ammonium to nitrite (nitritation), and with the nitrite AnAOB oxidize the residual ammonium to form dinitrogen gas and some nitrate (anammox). Additional aerobic nitrite oxidation to nitrate (nitratation) by nitrite-oxidizing bacteria (NOB) lowers the nitrogen removal efficiency, but it can, for instance, be prevented at low dissolved oxygen (DO) levels because the oxygen affinity of AerAOB is higher than that of NOB (16). Reactor configurations for the OLAND process can be based on suspended biomass growing in aggregates, like that in a sequencing batch reactor (SBR) (37) or a gas lift or upflow reactor (32). For suspended-growth systems there are two important challenges: biomass retention and equilibrated microbial activities.

High biomass retention efficiency is a prerequisite in anammox technologies because of the slow growth of AnAOB (33). In suspended biomass systems, settling properties determine the retention of biomass and are related to the microbial aggregate morphology (floc or granule) and size. Granules can be defined as compact and dense aggregates with an approximately spherical external appearance that do not coagulate under decreased hydrodynamic shear conditions and settle significantly faster than flocs (18). Toh and coworkers calculated a lower sludge volume index for aerobic granules than for aerobic flocs and also showed that there was an increase in the settling velocity with increasing granule size (35). Hence, in terms of physical properties, large granules are preferable for suspended-growth applications.

OLAND aggregate size not only influences settling properties but also affects the proportion of microbial nitrite production and consumption; lower AerAOB activity and higher AnAOB activity were observed with larger aggregates (25, 37).

* Corresponding author. Mailing address: Laboratory of Microbial Ecology and Technology (LabMET), Ghent University, Coupure Links 653, 9000 Ghent, Belgium. Phone: 32 9 264 59 76. Fax: 32 9 264 62 48. E-mail: Willy.Verstraete@UGent.be.

† Present address: Department of Chemical Engineering, Tokyo University of Agriculture and Technology, 2-24-16 Naka-cho, Koganei-shi, Tokyo 184-8588, Japan.

‡ Present address: Department of Chemical Engineering, School of Engineering, University of Santiago de Compostela, Rúa Lope Gómez de Marzoa, s/n, 15782 Santiago de Compostela, Spain.

▽ Published ahead of print on 30 November 2009.

TABLE 1. Overview of the three OLAND reactor systems from which suspended biomass samples were obtained

Parameter	Reactor A[a]	Reactor B[a]	Reactor C
Reactor type	SBR	SBR	Upflow reactor
Vol (m^3)	0.002	4.1	600
Reactor ht/diam ratio	0.9	4	0.5–0.8
Inoculum	OLAND biofilm	Activated sludge	Anammox granules
Wastewater	Synthetic	Domestic[b]	Industrial[c]
Influent ammonium concn (mg N $liter^{-1}$)	230–330	800	250–350
Nitrogen removal rate (g N $liter^{-1}$ day^{-1})	0.45,[d] 1.1[e]	0.65	1.3
Effluent nitrite concn (mg N $liter^{-1}$)	30–40[d]	5–10	5–10
Influent COD/effluent COD (mg $liter^{-1}$)	0/0	240/220	200/150
pH	7.4–7.8	7.4–7.6	8.0
Temp (°C)	35	25	30–35
DO level (mg O_2 $liter^{-1}$)	0.4–1.1	0.5–1.0	2.0–3.0
Mixing mechanism	Magnetic stirrer	Bladed impeller	Aeration
Biomass retention mechanism	MSV, >0.73 m h^{-1}	MSV, >1.4 m h^{-1}	Three-phase separator
Sampling time (months after start-up)	2[d]	8	30

[a] Aggregates settling at a rate higher than the minimum settling velocity (MSV) were not washed out of the sequencing batch reactors (SBR). The MSV was calculated by dividing the vertical distance of the water volume decanted per cycle by the settling time.
[b] Supernatant from a municipal sludge digestor.
[c] Effluent from a potato-processing factory pretreated with anaerobic digestion and struvite precipitation.
[d] Obtained at the end of a reactor start-up study (37).
[e] Obtained at the end of a reactor start-up study (9).

Theoretically, a microbial aggregate with equal nitrite production and nitrite consumption can remove ammonium autonomously, because of its independence from other aggregates for acquisition and conversion of nitrite. Hence, with an increasing aggregate size and thus with a decreasing ratio of nitrite production to nitrite consumption, three functional categories of aggregates can be distinguished: nitrite sources, autonomous nitrogen removers, and nitrite sinks. Because minimal nitrite accumulation is one of the prerequisites for high nitrogen removal efficiency in OLAND reactors, the presence of excess small aggregates is undesirable (9, 37).

Although large granular aggregates are desirable for biomass retention and activity balance, so far no formation mechanisms have been proposed for OLAND granules, in contrast to the well-studied anaerobic (13) and aerobic (1) granules. In order to determine general and environment-specific determinants for aggregate size and architecture, three suspended-growth OLAND reactors with different inoculation and operation (mixing and aeration) parameters were selected, and these reactors were designated reactors A, B, and C (Table 1). The first objective of this study was to gain more insight into the relationship between OLAND aggregate size, AerAOB and AnAOB abundance, and the activity balance. The second objective was to propose pathways for aggregation and granulation by relating (dis)similarities in aggregate size distribution, morphology, and architecture to differences in reactor inoculation and operation.

MATERIALS AND METHODS

Aerobic and anoxic batch activity tests. Representative mixed liquor samples were obtained from the three systems studied (reactors A, B, and C) (Table 1). The aerobic and anoxic ammonium-oxidizing activities were determined on the day after biomass was harvested to prevent storage effects. Depending on the sample, the biomass was sieved using various pore sizes (0.10, 0.25, 0.50, 1.0, 1.6, and 2.0 mm) and washed with phosphate buffer (100 mg P $liter^{-1}$, pH 8) to remove residual dissolved (in)organic compounds. The aerobic and anoxic tests used have been described previously in detail (38). In short, biomass was incubated in an Erlenmeyer flask with ammonium as the substrate for the aerobic activity tests. For the anoxic tests, biomass incubation was performed in a gas-tight anoxic serum flask with ammonium and nitrite as substrates. During incubation, liquid samples were taken over time and used for ammonium, nitrite, and nitrate analyses. After incubation, the biomass was analyzed for volatile suspended solids (VSS), which allowed expression of the activities as specific rates.

FISH. Fluorescent *in situ* hybridization (FISH) was performed to identify and visualize AerAOB, NOB, and AnAOB and to quantify AerAOB and AnAOB. Biomass was fixed in a 4% paraformaldehyde solution for 4 h at 4°C. Large aggregates were embedded in OCT compound, cut into 20-μm slices with a cryomicrotome (−20°C), and attached to poly-L-lysine coated slides. FISH was performed as described by Amann and coworkers (4). Specific probes and targets are shown in Table 2. The qualitative or quantitative presence of a target was evaluated by combining a specific probe with an equimolar mixture of EUB338I, EUB338II, and EUB338III targeting all bacteria (21) and 4′,6′-diamidino-2-phenylindole (DAPI) targeting all DNA-containing cells. The probe fluorochromes used were FLUO, Cy3, and Cy5. For quantification and visualization of the architecture, image acquisition was performed with a Leica TCM SP5 confocal laser scanning microscope (CLSM) (Leica Microsystems, Wetzlar, Germany). Ten CLSM image stacks (depth, 10 μm; three heights) were analyzed with Daime software (8), and the percentage of AerAOB and AnAOB was calculated by determining the ratio of the specific bacterial biovolume to the total bacterial biovolume. The architecture was also examined with a Zeiss Axioskop 2 Plus epifluorescence microscope (Carl Zeiss, Jena, Germany). If necessary, colors were digitally changed to green for AerAOB, blue for NOB, and red for AnAOB for consistency.

Staining of EPS. Concanavalin A, calcofluor white, fluorescein, and Nile red were applied to granule sections to target extracellular α-polysaccharides, β-polysaccharides, proteins, and lipids, respectively (7). Also, incubation with wheat germ agglutinin (for α-polysaccharides) at a concentration of 0.5 mg ml^{-1} was performed for 20 min at room temperature in the dark. The dyes were tested separately with granule sections that were previously stained using FISH. Probe fluorochromes were chosen to avoid interference with the fluorescence channel occupied by the extracellular polymeric substance (EPS) dye tested.

SEM and TEM. Scanning electron microscopy (SEM) and transmission electron microscopy (TEM) were performed with granules (diameter, >1 mm) from reactors A and C, using chemical fixation (SEM and TEM) and Epon embedding (TEM). The procedure described by Mast and coworkers was followed (22), except that TEM imaging was performed with a 120-kV Technai Spirit transmission electron microscope (FEI, Eindhoven, the Netherlands). Measurements on the electron micrographs were performed with ImageJ software (open source). The EPS area was determined after digital removal of the EPS with Adobe Photoshop CS 2 (Adobe, San Jose, CA) in a manually contoured group of cells (see Fig. 2E). The percentage of EPS was calculated by dividing the area of white pixels by the area of all contoured pixels. Intercellular distances were determined by determining the average of the minimum distances between a cell wall and the walls of neighboring cells (see Fig. 2F).

TABLE 2. Overview of the FISH probes and results for identification of AerAOB, ammonium-oxidizing archaea, NOB, and AnAOB[a]

Group	Probe(s)	Target(s)	Detection in[b]: Reactor A	Reactor B	Reactor C
AerAOB	Nso1225 and Nso190	Betaproteobacterial AerAOB	+	+	+
	Nse1472	*Nitrosomonas europaea, Nitrosomonas eutropha*, and *Nitrosomonas halophila*	+	+	+
	NmV	*Nitrosococcus mobilis* ("*Nitrosomonas*") lineage	−	−	−
	Nmo218	*Nitrosomonas oligotropha*	−	−	−
	Nsv443	*Nitrosospira* spp.	−	−	−
Ammonium-oxidizing archaea	Arc915	*Archaea*	−	−	−
	Cren537	*Crenarchaeota*	−	−	−
NOB	NIT3 and competitor probe	*Nitrobacter* spp.	−	−	−
	Ntspa662 and competitor probe	*Nitrospira* spp.	−	+	+
AnAOB	PLA46	*Planctomycetes*	+	+	+
	Amx820	"*Candidatus* Brocadia" and "*Candidatus* Kuenenia"	+	+	+
	Sca1309	"*Candidatus* Scalindua"	−	−	−

[a] In most cases probe sequences and formamide concentrations were used as described for probeBase (20); for the equimolar mixture of Nso1225 and Nso190, 35% formamide was used (30).
[b] +, detected; −, not detected.

Chemical analyses. Nitrite and nitrate contents were determined with a 761 compact ion chromatograph equipped with a conductivity detector (Metrohm, Zofingen, Switzerland). Ammonium content (Nessler method), chemical oxygen demand (COD) (dichromate method), and VSS content (weighing and drying) were determined using standard methods (12). pH was measured potentiometrically, and the DO concentration and water temperature were monitored with a COM381 DO meter (Endress-Hauser, Reinach, Switzerland).

RESULTS

Aggregate size and activity. The three types of suspended biomass (biomasses in reactors A, B, and C) (Table 1) had different morphologies and size distributions. The biomass in reactor A consisted of two fractions with different sizes: granular aggregates, all of which were more than 1 mm in diameter (Fig. 1A.1), and floccular aggregates, which were collected with a 0.10-mm sieve (Fig. 1A.2). The particle sizes for the biomass in reactor B were less divergent, and the particles were divided into four size classes (Fig. 1D). Since 90% of the particles in the biomass in reactor C were larger than 1 mm, additional size classes were created for this biomass, so that we ended up with six classes.

The rate of activity and the abundance of the AerAOB decreased with increasing aggregate size, whereas the opposite was true for the AnAOB activity and abundance (Table 3). These AerAOB and AnAOB trends were observed for all three reactor systems. In reactors A and B, no NOB activity was detected. In reactor C, the NOB activity decreased with increasing size starting at 0.25 mm. To evaluate the autotrophic nitrite accumulation potential of an aggregate or a mixture of aggregates, a dimensionless nitrite accumulation rate ratio (NARR) was calculated by dividing the net nitrite production rate by the nitrite consumption rate (equation 1):

$$\mathrm{NARR} = \frac{\text{AerAOB } NO_2^- \text{ production rate} - \text{NOB } NO_2^- \text{ consumption rate}}{\text{AnAOB } NO_2^- \text{ consumption rate}} \quad (1)$$

Large biomass A (diameter, >1.0 mm) and C (diameter, >0.50 mm) aggregates had NARR values close to 1 (Table 3). For all reactor systems the highest NARR values included the smallest aggregate size class, whereas the lowest NARR values were obtained for the larger reactor B aggregates (diameter, >0.25 mm) (Table 3). Taking into account the relative abundance of each size class, the NARR values for the mixed biomass were 2.3 for reactor A, 1.2 for reactor B, and 0.93 for reactor C.

Dominant autotrophs (FISH). In the three reactor systems, the dominant AerAOB belonged to *Nitrosomonas europaea*, *Nitrosomonas eutropha*, and *Nitrosomonas halophila* (Table 2), whose signals overlapped those of all betaproteobacterial AerAOB. No *Archaea* or *Crenarchaeota* were detected (Table 2), indicating that archaeal ammonium oxidizers did not contribute to aerobic ammonium oxidation. The NOB *Nitrospira* spp. were found in reactors B and C (Table 2), but in case of reactor B the activity tests showed that the few *Nitrospira* sp. microcolonies detected had a limited effect on the overall nitrogen conversion (Table 3). For all three systems, all *Planctomycetes* cells detected with probe PLA46 corresponded to the AnAOB "*Candidatus* Brocadia" and "*Candidatus* Kuenenia" (Table 2).

Autotrophic aggregate architecture. The appearance of aggregates differed in different reactor systems, especially for the large aggregates, which were globular and rigid granules in reactors A (Fig. 1A.1) and C (Fig. 1F) and planar and flexible film-like structures in reactor B (Fig. 1D.1).

Thin sections showed that the reactor A granular architecture consisted of an AerAOB rim and many internal parallel AerAOB layers in which AnAOB zones were embedded (Fig. 1B). The thickness of the AerAOB rim ranged from 24 ± 6 to 43 ± 8 μm (n = 15), and lower AerAOB cell density was observed toward the inside of a granule (Fig. 1C.1). Internal AerAOB bands were 16 ± 4 μm thick (n = 32), with spaces 14 ± 5 μm thick between them (n = 32). The different direc-

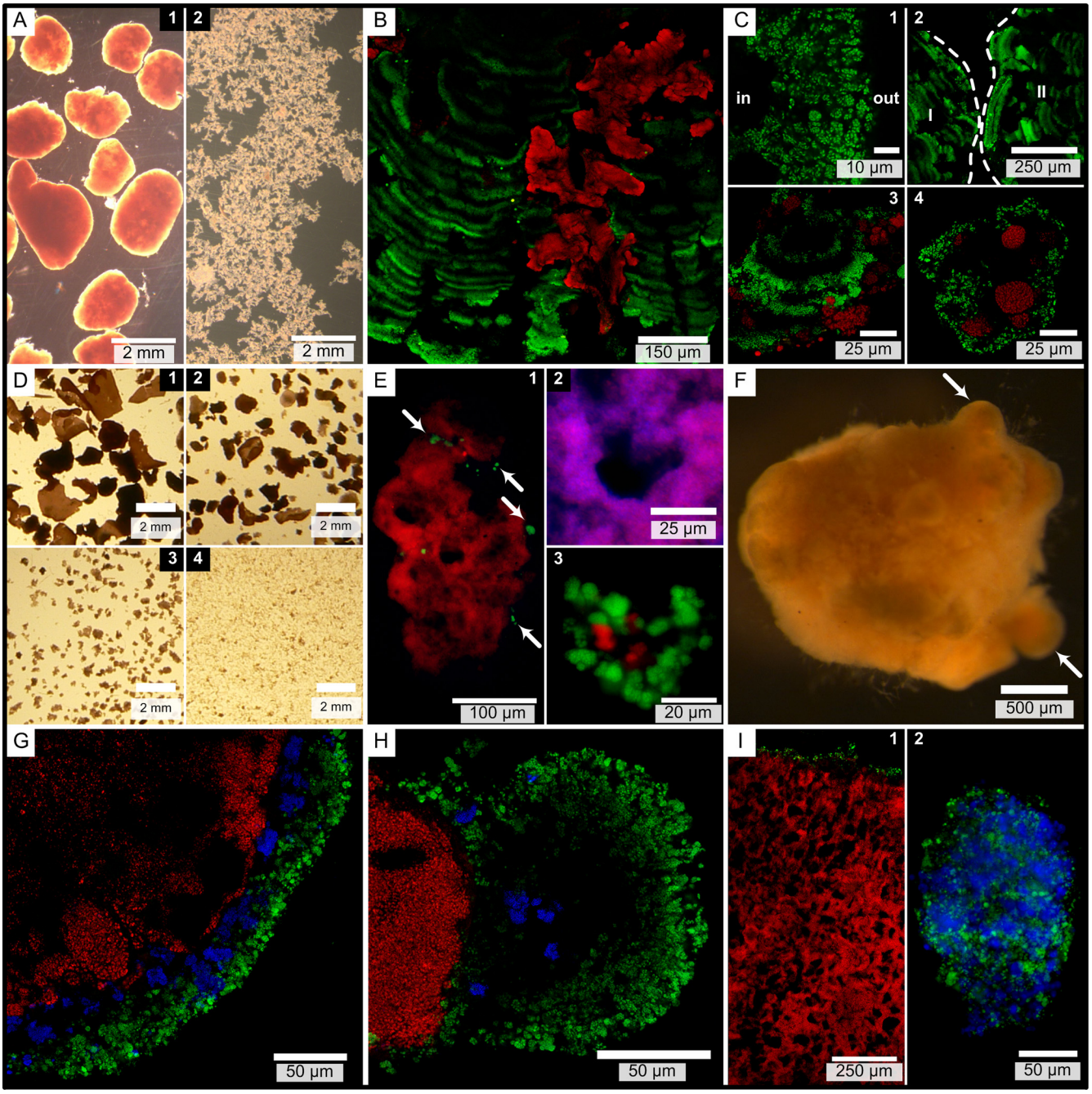

FIG. 1. Micrographs of biomass from reactors A (A to C), B (D to E), and C (F to I). In the FISH images, AerAOB (with probes Nso1225 and Nso190) are green, *Nitrospira* spp. (with probe Ntspa662) are blue, and AnAOB (with probe Amx820) are red. FISH micrographs were acquired with a confocal laser scanning microscope (B, C, G, H, and I.1) or an epifluorescence microscope (E and I.2). (A) Two size fractions in biomass from reactor A. (B) Granule with pleomorphic AnAOB zones embedded in parallel AerAOB bands. (C.1) AerAOB rim with the granule core to the left (indicated by "in"). (C.2) Different directions of parallel AerAOB bands in cosectioned granules (granules I and II, indicated by dashed lines). (C.3) Parallel AerAOB bands in OLAND biofilm. (C.4) Floc with AerAOB and AnAOB microcolonies. (D) Four size fractions in biomass from reactor B. (E.1) Large aggregate with some AerAOB microcolonies (arrows) on the AnAOB core. (E.2) Anoxic void with AnAOB and all cells (DAPI, blue) (red + blue = magenta). (E.3) Floc with AerAOB and AnAOB microcolonies. (F) Reactor C granule with lobate extrusions (arrows). (G) Three-layer granule stratification with AerAOB, *Nitrospira* spp., and AnAOB. (H) Lobate granule extrusion. (I.1) Ubiquity of anoxic void spaces. (I.2) Floc with AerAOB and NOB microcolonies.

tions of parallel AerAOB bands in cosectioned granules show that the bands were not a compaction artifact of cryomicrotome sectioning (Fig. 1C.2). Similar internal AerAOB bands were observed in nonsectioned biofilms from an OLAND rotating biological contactor (Fig. 1C.3). The AnAOB were heterogeneously spread over the granule section, appearing as spherical microcolonies (data not shown) or as pleomorphic zones (Fig. 1B).

In contrast to the results for reactor A, AnAOB were not

TABLE 3. Activity of AerAOB, NOB, and AnAOB by aggregate size, as determined in batch activity tests ($n = 1$ for reactor A, $n = 3$ for reactor B, and $n = 3$ for reactor C)[a]

Parameter	Reactor A biomass (by aggregate size [mm])		Reactor B biomass (by aggregate size [mm])				Reactor C biomass (by aggregate size [mm])					
	0.1–1.0	>1.0	0.1–0.25	0.25–0.5	0.5–1.0	>1.0	0.1–0.25	0.25–0.5	0.5–1.0	1.0–1.6	1.6–2.0	>2.0
% of total VSS	43	57	77	10	6	7	2.7	1.0	6.7	35	35	20
Rate of NH_4^+ consumption by AerAOB (mg NH_4^+-N g VSS^{-1} day^{-1})	426	110	191 ± 20	85 ± 2	32 ± 2	21 ± 13	1,040 ± 86	200 ± 35	218 ± 21	209 ± 12	173 ± 31	159 ± 17
Rate of NO_3^- production by NOB (mg NO_3^--N g VSS^{-1} day^{-1})	0	0	0	0	0	0	37 ± 15	72 ± 8	56 ± 11	47 ± 1	45 ± 11	36 ± 2
Rate of NH_4^+ consumption by AnAOB (mg NH_4^+-N g VSS^{-1} day^{-1})	36	133	99 ± 5	172 ± 2	159 ± 5	191 ± 8	5.6 ± 4.6	103 ± 26	163 ± 11	156 ± 13	161 ± 15	171 ± 9
NARR	10	0.70	1.7	0.44	0.18	0.10	158	1.1	0.88	0.92	0.70	0.63
AerAOB abundance (%)	80 ± 7	36 ± 9	25 ± 4	ND[b]	ND	1.1 ± 0.6	29 ± 11	ND	ND	ND	4.9 ± 1.5	ND
AnAOB abundance (%)	6.0 ± 0.9	22 ± 8	21 ± 6	ND	ND	85 ± 8	1.3 ± 8.9	ND	ND	ND	69 ± 7	ND

[a] The ratio of AnAOB nitrite consumption to ammonium consumption differed slightly in the reactor systems (for reactor A, 1.17; for reactor B, 1.11 ± 0.02; for reactor C, 1.13 ± 0.02), but it was not affected by the aggregate size. Calculation and interpretation of the NARR are described in the Results. AerAOB abundance and AnAOB abundance were determined by FISH and are expressed as percentages of the total bacterial volume. Activity and abundance data are expressed as averages ± standard deviations.

[b] ND, not determined.

surrounded by AerAOB in large reactor B aggregates. Sections showed an AnAOB zone with only some scattered AerAOB microcolonies on the edge (Fig. 1E.1). Irregularly shaped void spaces that were up to ca. 50 by 50 μm occupied 13% ± 5% ($n = 10$) of the combined AnAOB and void area. No cells were present in the voids (Fig. 1E.2).

Reactor C granules consisted of an AerAOB rim similar to that of reactor A granules and then a *Nitrospira* sp. layer and an AnAOB core (Fig. 1G). The AerAOB rim ranged from 20 ± 7 to 35 ± 12 μm thick ($n = 15$), and the combined aerobic layer (AerAOB and NOB) ranged from 30 ± 11 to 65 ± 17 μm thick ($n = 15$), which is roughly 20 μm thicker than the AerAOB rim of reactor A granules. The lobate granule extrusions observed (Fig. 1F) consisted primarily of AerAOB (Fig. 1H). Similar to the reactor B findings, the AnAOB zone contained irregularly shaped voids or channels up to ca. 50 by 150 μm (Fig. 1I.1), which occupied 17% ± 4% ($n = 10$) of the combined AnAOB and void zone. No cells were present in the voids (data not shown).

In the smallest biomass fractions (diameter, 0.10 to 0.25 mm), the autotrophs appeared mostly in spherical microcolonies. In reactors A and B, AnAOB clusters were located close to AerAOB clusters (Fig. 1C.4 and 1E.3), and the AnAOB abundance was greater in reactor B than in reactor A (Table 3). In reactor C, almost no AnAOB were detected (Table 3), and *Nitrospira* sp. microcolonies were larger than and located close to AerAOB microcolonies (Fig. 1I.2).

Granular surface, intercellular organization, and EPS. Granular aggregates from reactors A and C (diameter, >1 mm) were used to study cell sizes, intercellular distances, and EPS amount and composition. SEM showed that the granular surface was heterogeneous and rough with irregular shapes like lobate extrusions and cavities (Fig. 2A, B, and C).

In TEM images, AerAOB could be recognized by the presence and structure of the intracytoplasmic membranes (40), and AnAOB could be recognized by their typical cytoplasmic compartmentalization (19). AerAOB cells were smaller than AnAOB cells (Table 4). The predominant AerAOB cell ultrastructure was the ultrastructure of the genus *Nitrosomonas*, with intracytoplasmic membranes along the periphery of the cell, which is in agreement with the FISH detection of *N. europaea*, *N. eutropha*, and *N. halophila*.

In general, around 50% of the AerAOB and AnAOB zones consisted of EPS (Table 4). Only in reactor A granules was there a difference between AerAOB cells present in globular microcolonies and AerAOB cells appearing ungrouped. The latter AerAOB cells produced significantly more EPS, and the intercellular distances exceeded the cell sizes. Scattered AerAOB were observed in the granule rim toward the core (Fig. 2D) and on the internal AerAOB bands (data not shown).

In contrast to AerAOB EPS (Fig. 2E), AnAOB EPS differed visually from the EPS surrounding the microcolony (Fig. 2F). Fluorescent dyes for α-polysaccharides, proteins, and lipids attached to both the AerAOB and AnAOB zones, as shown by FISH. Only calcofluor white for β-polysaccharide detection did not bind to the AnAOB zone (Fig. 2G.1 and 2G.2).

Phages and protozoans. Some damaged AerAOB cells were invaded by icosahedral virions (Fig. 2H.1). These bacteriophages were regularly shaped and more or less the same size (58 ± 3 nm; $n = 130$) and had an outer capsid layer on the phage head (Fig. 2H.2). In contrast, phages were never observed in AnAOB. Further, similar globular protozoans with an average diameter of 6.1 ± 1.3 μm ($n = 43$) were observed in reactor A and C granules (Fig. 2I). The presence of eukaryotes in AnAOB zones (Fig. 2J) indicates that oxygen was not a strict metabolic requirement for them. The protozoans had a clear cell coat (thickness, ca. 100 nm) and a central, presumably nuclear region (Fig. 2K.1). It is not clear whether cytoplasmic particles with and without internal membranes (Fig. 2K.2) were regular eukaryotic structures or bacteria which were hypobiotic or ingested.

DISCUSSION

The first objective of this study was to relate the AerAOB and AnAOB abundance and the activity balance to the size of

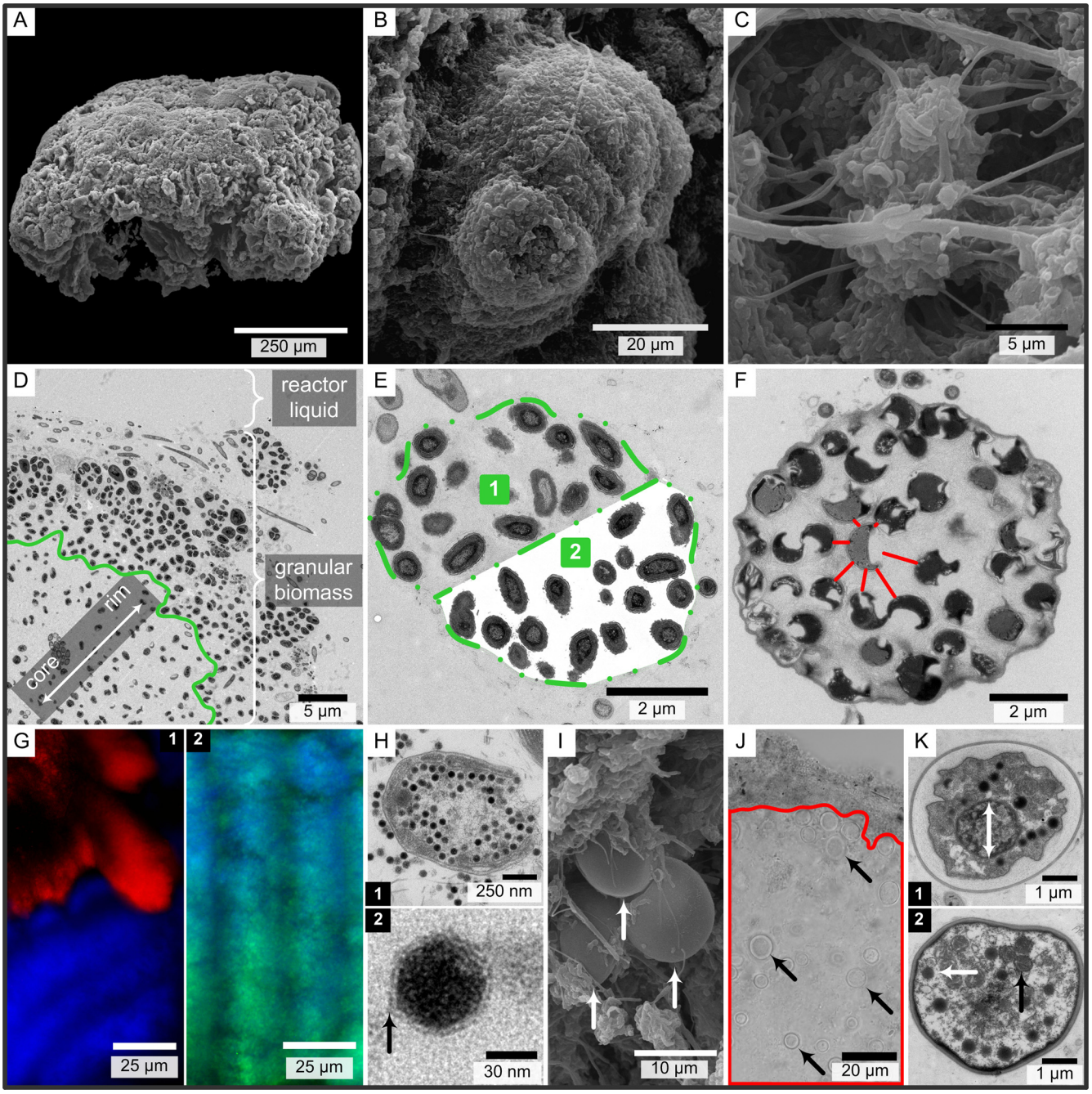

FIG. 2. SEM (A to C and I), TEM (D to F, H, and K), light (J), and fluorescence (G) micrographs of reactor A (A, B, D, E, G, H, and K) and C (C, F, I, and J) granules (diameter, >1 mm). (A) One granule. (B) Lobate extrusion covered with some filaments. (C) Cavities with various filaments and rods. (D) Separation of the more clustered AerAOB from the more scattered AerAOB in the granule rim, indicated by the green line. (E) AerAOB microcolony with extracellular polymeric substances (EPS) (area 1) and with digital removal of EPS (area 2). (F) AnAOB microcolony showing the distinct AnAOB EPS matrix. Red lines indicate the cell distances for one cell. (G) Extracellular β-polysaccharides (calcofluor white) (blue) are not associated with AnAOB (FISH) (red) (G.1) but are associated with AerAOB (FISH) (green; green + blue = cyan) (G.2). (H.1) Bacteriophage replication in an AerAOB cell. (H.2) Outer capsid layer of a phage head. (I) Protozoans (arrows) on a granule surface. (J) Protozoans (arrows) in the AnAOB zone (red line). The granule rim is at the top. (K) Protozoan ultrastructure with a central, presumably nuclear region (K.1) and intracellular particles with (black arrow) and without (white arrow) internal membranes (K.2).

OLAND aggregates. The activity and abundance of AerAOB were lower with increasing aggregate size, and the activity and abundance of AnAOB were higher with increasing aggregate size. The activity balance was evaluated using nitrite production and consumption and was condensed into the dimensionless parameter NARR. The validity of NARR depends on two assumptions: (i) the ratio of the activity rates determined for a batch can be extrapolated to the *in situ* reactor activity and (ii)

TABLE 4. Overview of measurements on TEM micrographs for reactor A and C granules[a]

Parameter	Reactor A biomass				Reactor C biomass	
	AerAOB			AnAOB	AerAOB	AnAOB
	Overall	Clustered	Scattered			
Cell length (nm)	852 ± 199			1,213 ± 253	834 ± 191	1,055 ± 193
Cell length/cell width	1.62 ± 0.46 (240)			1.43 ± 0.39 (218)	1.40 ± 0.31 (194)	1.34 ± 0.24 (236)
EPS area (%)		49 ± 9 (965)	78 ± 6 (934)	42 ± 11 (1,242)	57 ± 14 (1,113)	47 ± 11 (860)
Cell distances (nm)		254 ± 231 (445)	989 ± 764 (590)	574 ± 472 (410)	330 ± 262 (577)	313 ± 259 (404)

[a] The amount of EPS is expressed as a percentage of the area examined (cells and EPS). The numbers in parentheses are the numbers of units measured (numbers of cells for the EPS area).

in case of NOB activity NOB preferentially consume the nitrite before the AnAOB consume it because of their close proximity to the nitrite producers (AerAOB). Based on the NARR definition (equation 1), the functional categories nitrite sources, autonomous nitrogen removers, and nitrite sinks can be attributed to NARR values which are considerably less than 1, around 1, and considerably more than 1, respectively. The relationship between the functional category and the size of an aggregate was dependent on the system examined. Reactor A and C granules had an NARR value around 1 and hence could autonomously remove nitrogen without excessive aerobic nitrite production or severe anoxic nitrite limitation. Similarly, the large flocs obtained by Nielsen and coworkers (diameter, >0.50 mm) were autonomous nitrogen removers, based on their NARR value of 1.1 (25). In contrast, large reactor B aggregates were nitrite sinks, and all of the small aggregates were nitrite sources. This suggests that nitrite sources had to feed nitrite sinks for nitrogen removal in reactor B to occur. An NARR was also calculated for the mixture of aggregate sizes. The high value for reactor A (NARR, 2.3) corresponded well to the relatively high nitrite levels in the reactor effluent (Table 1). Overall, the NARR can be determined easily and is a useful tool for evaluating the OLAND activity balance of an aggregate (mixture) in a dimensionless way.

The second objective of this study was to determine specific effects of reactor inoculation and operation on the observed biomass properties in order to propose pathways for aggregation (single cells to aggregates) and granulation (flocs to granules). Minor differences in biodegradable organic carbon in the influent were assumed to have a minor effect on autotrophic activity ratios and architecture, since a change in the influent from synthetic to real digested wastewater has previously been shown not to influence the autotrophic community significantly (39).

Cell aggregation was ensured in the systems examined (Table 1), and the minimum settling velocity (SBR) or three-phase separator (upflow reactor) selected for biomass with sufficient settling ability (i.e., aggregated cells). Note that the absence of such a selection pressure can result in a suspension of nonaggregated, single cells (36). EPS formation is a basic requirement for cell aggregation, as this biogenic glue immobilizes single cells in multicellular aggregates (flocs or granules). In summary, AerAOB and AnAOB accounted for 58 to 74% of the bacteria in OLAND granules (Table 3), and EPS occupied at least ~50% of the autotrophic space (Table 4). Although autotrophic EPS is often overlooked in studies (3), its volumetric presence cannot be neglected in OLAND granules. The measured intercellular distances and relative EPS areas are very valuable input data for constructing realistic mathematical models for biofilms or granules which represent cells as individuals (15). In EPS secreted by AnAOB, β-polysaccharides were not present, as shown by fluorescent staining, whereas these EPS compounds are very important for maintaining the structural strength of aerobic granules (2). Note that the peculiar EPS around AnAOB cells might protect AnAOB from phages, which were observed only inside AerAOB.

For OLAND granulation, the core driving force is not selective settling, in contrast to what has been observed for aerobic (1) and anaerobic (13) granulation, because OLAND granules were previously obtained at a low settling rate (0.3 to 0.7 m h^{-1}) (14, 37). So far, the exact physical or chemical triggers for OLAND granulation are not clear, but sufficient hydrodynamic shear may be necessary, as it is in aerobic granulation (20). The macroscopic semispherical shape of granules can be considered the result of three-dimensional aggregate expansion by microbial growth based on species-specific physiology (e.g., DO affinity or inhibition) combined with globular surface erosion by hydrodynamic shear. Based on this physiology, mature OLAND granules should contain AerAOB in the aerobic rim and AnAOB in the anoxic core, resulting in a symmetric architecture, as observed in reactor C granules. As a conceptual basis for future experimental validation, previous findings for aerobic and anaerobic granulation were combined with our morphological observations to propose a scheme for OLAND granulation states and pathways (Fig. 3). Small granules are expected to expand to large granules due to microbial growth, whereas flocs can originate from granules due to shear-related surface erosion. Further, large granules are thought to replicate by two pathways, division and budding. Since the size of reactor C granules never exceeded 5 mm, granule division occurs at a certain size, probably due to internal decay and subsequent shear on or collisions of weakened granules, as described previously for anaerobic granulation (5). In the daughter aggregates, growth of the residual AerAOB, as well as attachment of AerAOB from flocs, could lead to a new complete AerAOB rim. Lobate granule extrusions (Fig. 1F and H) indicated that there is a budding pathway, which has not been reported previously to our knowledge. Growth of similar biofilm extrusions is typically considered the result of limitation of transfer of substrate (29), in our case DO for the AerAOB. It is proposed that once the outgrowths reach a certain size, they detach and finally form a new granule. Below, the effects of inoculum structure (reactor A), hydraulic flow pattern (reactor

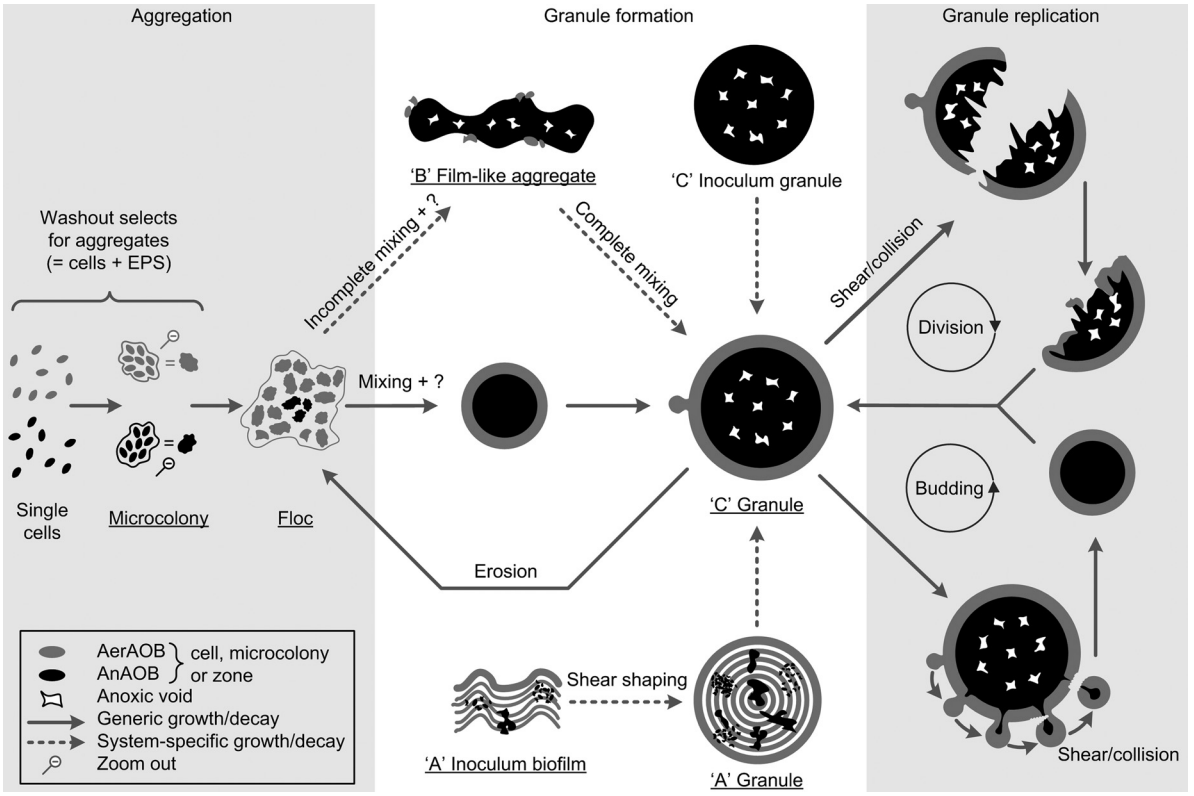

FIG. 3. Overview of the proposed pathways for OLAND aggregation and granulation, including granule replication by division and budding. The biomass morphologies observed in this study are underlined. NOB are not considered due to a low dissolved oxygen level. The arrows indicate growth and/or decay based on species-specific physiology, and the labels for arrows indicate additional roles of hydrodynamic shear or the mixing regimen. A possible, unknown granulation trigger is indicated by a question mark. The pathways are described more in detail in the Discussion.

B), DO concentration (reactor C), and AnAOB decay (reactors B and C) on aggregate architecture are clarified.

In reactor A granules, internal AerAOB layers (Fig. 1B) were probably derived from the inoculum (biofilm grown on rotating disks) since the same structures were observed there (Fig. 1C.3). The lowest aerobic specific activity was found for reactor A granules (306 mg N g^{-1} AerAOB VSS^{-1} day^{-1}), indicating that the AerAOB in the anoxic core could not grow aerobically. Compared to the anoxic activity of the inoculum biofilm, the anoxic activity of the granules was 6-fold higher (37), showing that there was AnAOB growth in the anoxic granule core. When these facts were combined with the early biomass harvest (Table 1), reactor A granules were considered to be structurally immature. Further central AnAOB growth, generating expanding pleomorphic zones from spherical microcolonies, would push aerobically inactive AerAOB bands outward, where extrusions would be removed by hydrodynamic shear and aggregate collisions. In the longer term, the mature granule architecture would appear (Fig. 3).

The spatial distribution of dissolved oxygen determines where AerAOB and AnAOB can grow, since oxygen is an AerAOB substrate and an AnAOB inhibitor (34). In reactor systems A and C, the granular aerobic rim could create anoxic conditions on a micro scale (50 to 100 μm). In contrast, large reactor B aggregates were not surrounded by AerAOB, probably due to oxygen gradients on a macro (reactor) scale. Gentle impeller mixing and the high height/diameter ratio of the reactor (Table 1) were factors that resulted in heterogeneous, incomplete mixing. Large aggregates could settle in hydraulically "dead," anoxic reactor corners, allowing AnAOB growth. In the short term, stressing the system with enhanced, homogeneous mixing is expected to inhibit some of the AnAOB and decrease nitrogen removal. In the longer term, however, growth of an AerAOB rim would allow AnAOB activity and growth and development of a globular morphology (Fig. 3).

In reactor C, the relatively high DO levels (Table 1) can explain the high rates of NOB activity for all size classes, as well as the low rates of AnAOB activity in the smallest aggregates. NOB activity accounted for 21% of the AerAOB rate in the overall reactor C sample. In the likely event that the NOB oxygen affinity constant exceeded that of its AerAOB counterpart (16), a decrease in the DO level would outcompete the NOB, increasing the overall nitrogen removal efficiency. Further, a calculation based on the measured aerobic activity showed that a decrease in the DO concentration from 2.5 to 0.75 mg O_2 $liter^{-1}$ decreased the radial oxygen penetration depth in the smallest aggregates from 96 to 52 μm, assuming zero-order substrate uptake (28). The deep oxygen penetration at the high DO level explains the low AnAOB abundance (1%)

(Table 3), and the anoxic zones generated by a decrease in the DO concentration would allow AnAOB proliferation, lowering the extremely high NARR (158).

Besides species-specific growth, decay is also thought to play a role in the mature granule architecture. Large reactor B and C aggregates were AnAOB rich (85 and 69%), but their AnAOB-specific removal rates (224 and 233 mg N g^{-1} AnAOB VSS^{-1} day^{-1}) were at least two times lower than those in the other AnAOB-quantified biomass (430 to 605 mg N g^{-1} AnAOB VSS^{-1} day^{-1}). It follows that some of the AnAOB in AnAOB-rich aggregates were substrate limited. Subsequent decay could give rise to formation of voids occupying 13 to 17% of the anoxic zone. In contrast to voids observed in aerobic granules (18), no connections were seen between a void and the outside of a granule.

Overall, three suspended OLAND systems with comparable nitrogen removal rates and different inoculum and operation conditions showed different NARR distributions based on aggregate size. This corresponded well with the distributions of AerAOB and AnAOB abundances in each system. To obtain good nitrogen removal, no unique, optimal aggregate size distribution was required. Yet a decrease in the abundance of the smallest aggregates in the system can prevent nitrite accumulation, and an AerAOB rim, shielding the AnAOB from oxygen, results in more stress-resistant operation. Autotrophic EPS has been overlooked so far and might play an important role in the formation and strength of granules. Proposed granulation pathways were driven by growth and/or decay based on species-specific physiology and by a hydrodynamic shear and mixing regimen. Finally, a new budding mechanism is proposed here for granule replication. A follow-up study with independent variations in reactor inoculation and operation should confirm the findings obtained.

ACKNOWLEDGMENTS

This research was funded by a Ph.D. grant (Aspirant) for S.E.V. from the Fonds voor Wetenschappelijk Onderzoek (FWO) Vlaanderen, by a Ph.D. grant for H.D.C. from the Instituut voor de aanmoediging van innovatie door Wetenschap en Technologie (IWT) Vlaanderen (grant SB-81068), and by a postdoctoral contract for M.C. from the Xunta de Galicia (Isidro Parga Pondal program, grant IPP-08-37). Work at DTU was supported by research grant FTP-ReSCoBiR from the Danish Agency for Science Technology and Innovation (Research Council for Technology & Production, FTP).

We express our utmost gratitude to Wiebe Abma (Paques, Balk, the Netherlands) and Laure Graveleau (Degrémont, Rueil Malmaison, France) for their very kind provision of biomass. The molecular expertise of Diederik Vandriessche and Siska Maertens is acknowledged. We thank Mark van Loosdrecht, Laura van Niftrik, Eveline Volcke, Loïs Maignien, and Tom Hennebel for inspiring scientific discussions.

REFERENCES

1. **Adav, S. S., D. J. Lee, K. Y. Show, and J. H. Tay.** 2008. Aerobic granular sludge: recent advances. Biotechnol. Adv. **26:**411–423.
2. **Adav, S. S., D. J. Lee, and J. H. Tay.** 2008. Extracellular polymeric substances and structural stability of aerobic granule. Water Res. **42:**1644–1650.
3. **Alpkvist, E., C. Picioreanu, M. C. M. van Loosdrecht, and A. Heyden.** 2006. Three-dimensional biofilm model with individual cells and continuum EPS matrix. Biotechnol. Bioeng. **94:**961–979.
4. **Amann, R. I., L. Krumholz, and D. A. Stahl.** 1990. Fluorescent-oligonucleotide probing of whole cells for determinative, phylogenetic, and environmental studies in microbiology. J. Bacteriol. **172:**762–770.
5. **Beeftink, H. H., and P. Staugaard.** 1986. Structure and dynamics of anaerobic bacterial aggregates in a gas-lift reactor. Appl. Environ. Microbiol. **52:**1139–1146.
6. Reference deleted.
7. **Chen, M. Y., D. J. Lee, J. H. Tay, and K. Y. Show.** 2007. Staining of extracellular polymeric substances and cells in bioaggregates. Appl. Microbiol. Biotechnol. **75:**467–474.
8. **Daims, H., S. Lucker, and M. Wagner.** 2006. daime, a novel image analysis program for microbial ecology and biofilm research. Environ. Microbiol. **8:**200–213.
9. **De Clippeleir, H., S. E. Vlaeminck, M. Carballa, and W. Verstraete.** 2009. A low volumetric exchange ratio allows high autotrophic nitrogen removal in a sequencing batch reactor. Bioresour. Technol. **100:**5010–5015.
10. Reference deleted.
11. **Fux, C., and H. Siegrist.** 2004. Nitrogen removal from sludge digester liquids by nitrification/denitrification or partial nitritation/anammox: environmental and economical considerations. Water Sci. Technol. **50:**19–26.
12. **Greenberg, A. E., L. S. Clesceri, and A. D. Eaton.** 1992. Standard methods for the examination of water and wastewater. American Public Health Association, Washington, DC.
13. **Hulshoff Pol, L. W., S. I. de Castro Lopes, G. Lettinga, and P. N. L. Lens.** 2004. Anaerobic sludge granulation. Water Res. **38:**1376–1389.
14. **Innerebner, G., H. Insam, I. H. Franke-Whittle, and B. Wett.** 2007. Identification of anammox bacteria in a full-scale deammonification plant making use of anaerobic ammonia oxidation. Syst. Appl. Microbiol. **30:**408–412.
15. **Kreft, J. U., C. Picioreanu, J. W. T. Wimpenny, and M. C. M. van Loosdrecht.** 2001. Individual-based modelling of biofilms. Microbiology **147:**2897–2912.
16. **Laanbroek, H. J., and S. Gerards.** 1993. Competition for limiting amounts of oxygen between *Nitrosomonas europaea* and *Nitrobacter winogradskyi* grown in mixed continuous cultures. Arch. Microbiol. **159:**453–459.
17. Reference deleted.
18. **Lemaire, R., R. I. Webb, and Z. G. Yuan.** 2008. Micro-scale observations of the structure of aerobic microbial granules used for the treatment of nutrient-rich industrial wastewater. ISME J. **2:**528–541.
19. **Lindsay, M. R., R. I. Webb, M. Strous, M. S. Jetten, M. K. Butler, R. J. Forde, and J. A. Fuerst.** 2001. Cell compartmentalisation in planctomycetes: novel types of structural organisation for the bacterial cell. Arch. Microbiol. **175:**413–429.
20. **Liu, Y., and J. H. Tay.** 2002. The essential role of hydrodynamic shear force in the formation of biofilm and granular sludge. Water Res. **36:**1653–1665.
21. **Loy, A., M. Horn, and M. Wagner.** 2003. probeBase: an online resource for rRNA-targeted oligonucleotide probes. Nucleic Acids Res. **31:**514–516.
22. **Mast, J., C. Nanbru, T. van den Berg, and G. Meulemans.** 2005. Ultrastructural changes of the tracheal epithelium after vaccination of day-old chickens with the La Sota strain of Newcastle disease virus. Vet. Pathol. **42:**559–565.
23. **Mulder, A.** 2003. The quest for sustainable nitrogen removal technologies. Water Sci. Technol. **48:**67–75.
24. Reference deleted.
25. **Nielsen, M., A. Bollmann, O. Sliekers, M. Jetten, M. Schmid, M. Strous, I. Schmidt, L. H. Larsen, L. P. Nielsen, and N. P. Revsbech.** 2005. Kinetics, diffusional limitation and microscale distribution of chemistry and organisms in a CANON reactor. FEMS Microbiol. Ecol. **51:**247–256.
26. Reference deleted.
27. Reference deleted.
28. **Perez, J., C. Picioreanu, and M. van Loosdrecht.** 2005. Modeling biofilm and floc diffusion processes based on analytical solution of reaction-diffusion equations. Water Res. **39:**1311–1323.
29. **Picioreanu, C., M. C. M. van Loosdrecht, and J. J. Heijnen.** 1998. Mathematical modeling of biofilm structure with a hybrid differential-discrete cellular automaton approach. Biotechnol. Bioeng. **58:**101–116.
30. **Pynaert, K., B. F. Smets, S. Wyffels, D. Beheydt, S. D. Siciliano, and W. Verstraete.** 2003. Characterization of an autotrophic nitrogen-removing biofilm from a highly loaded lab-scale rotating biological contactor. Appl. Environ. Microbiol. **69:**3626–3635.
31. Reference deleted.
32. **Sliekers, A. O., K. A. Third, W. Abma, J. G. Kuenen, and M. S. M. Jetten.** 2003. CANON and anammox in a gas-lift reactor. FEMS Microbiol. Lett. **218:**339–344.
33. **Strous, M., J. J. Heijnen, J. G. Kuenen, and M. S. M. Jetten.** 1998. The sequencing batch reactor as a powerful tool for the study of slowly growing anaerobic ammonium-oxidizing microorganisms. Appl. Microbiol. Biotechnol. **50:**589–596.
34. **Strous, M., E. van Gerven, J. G. Kuenen, and M. Jetten.** 1997. Effects of aerobic and microaerobic conditions on anaerobic ammonium-oxidizing (anammox) sludge. Appl. Environ. Microbiol. **63:**2446–2448.
35. **Toh, S. K., J. H. Tay, B. Y. P. Moy, V. Ivanov, and S. T. L. Tay.** 2003. Size-effect on the physical characteristics of the aerobic granule in a SBR. Appl. Microbiol. Biotechnol. **60:**687–695.
36. **van der Star, W. R. L., A. I. Miclea, U. van Dongen, G. Muyzer, C. Picioreanu, and M. C. M. van Loosdrecht.** 2008. The membrane bioreactor: a novel tool to grow anammox bacteria as free cells. Biotechnol. Bioeng. **101:**286–294.
37. **Vlaeminck, S. E., L. F. F. Cloetens, M. Carballa, N. Boon, and W. Verstraete.**

2009. Granular biomass capable of partial nitritation and anammox (vol 58, pg 1113, 2008). Water Sci. Technol. **59:**609–617.
38. **Vlaeminck, S. E., J. Geets, H. Vervaeren, N. Boon, and W. Verstraete.** 2007. Reactivation of aerobic and anaerobic ammonium oxidizers in OLAND biomass after long-term storage. Appl. Microbiol. Biotechnol. **74:**1376–1384.
39. **Vlaeminck, S. E., A. Terada, B. F. Smets, D. Van der Linden, N. Boon, W. Verstraete, and M. Carballa.** 2009. Nitrogen removal from digested black water by one-stage partial nitritation and anammox. Environ. Sci. Technol. **43:**5035–5041.
40. **Watson, S. W., E. Bock, H. Harms, H. P. Koops, and A. B. Hooper.** 1989. Nitrifying bacteria, p. 1808–1834. *In* J. T. Staley, M. T. Bryant, N. Pfennig, and J. G. Holt (ed.), Bergey's manual of systematic bacteriology, vol. 3. The Williams & Wilkins Co., Baltimore, MD.